Numerical simulation of asymmetric dual-core fiber with large group-velocity dispersion*

YANG Jian-fang (杨建芳) **and WANG Chun-can** (王春灿)**

Key Laboratory of All Optical Network and Advanced Telecommunication Network, Ministry of Education, Institute of Lightwave Technology, Beijing Jiaotong University, Beijing 100044, China

(Received 16 February 2020; Revised 29 March 2020)

The asymmetric dual-core fiber (ADCF) is proposed to obtain large group velocity dispersion (GVD) because of the coupling effects between the fundamental modes of the central core and high-order modes of the side core. The supermodes of the ADCF can provide anomalous- and normal-GVD profiles with large peak values at the maximum dispersion wavelengths. The maximum dispersion wavelengths can be shifted in the wavelength window of 1 550 nm by properly tuning the refractive indexes and diameters of the cores or spacing between the two cores. Furthermore, the numerical results show that the ADCF with the normal-GVD supermode 1 can be employed in the pulse broadening, where the broadening factor can reach more than 30 without pulse distortion from nonlinear effects.

Document code: A **Article ID:** 1673-1905(2021)02-0096-6

DOI https://doi.org/10.1007/s11801-021-0026-5

The transmission data rates of the long-haul optical communication system are restricted seriously by the accumulated dispersion in the optical links. Large dispersion fibers with low insertion loss are strongly required for dispersion compensation in these systems. Several all-fiber solutions have been proposed to obtain large group velocity dispersion (GVD), such as chirped fiber Bragg grating (FBG), dispersion compensation fibers (DCFs) and photonic crystal fibers (PCFs). For example, it has been demonstrated experimentally that the chirped fiber Bragg grating (FBG) can be used for dispersion compensations due to its large dispersion and negligible nonlinear effects. However, an optical circulator or a fiber coupler is required as an additional component with associated insertion loss because it operates in the reflection mode[1-3]. The DCFs consisting of two spatially separated asymmetric concentric cores can achieve large GVD due to the coupling between the inner and outer cores and support single-mode operations with high refractive index cores and small core diameters[4-6]. Besides, the DCFs have low sensitivity to environmental influence such as temperature and vibration. The dual-concentric-core photonic crystal fibers (DCPCF) formed by raising the refractive index of one of the cladding's rings can provide large GVD at the desired wavelength by properly tuning the geometrical parameters[7-11]. Moreover, a waveguide based on a structure of coupled asymmetric subwavelength-diameter wires, i.e., an optical nanofiber and a GaAs nanowire, has been proposed to realize a high negative dispersion up to -4.5×10^6 ps/(nm·km)[12]. Thus, there is a need in identifying a simple, compact, easily spliced with single-mode fiber, highly efficient devices that exhibit tunable GVD and operate in transmission. Such a structure should find applications for ultrafast optical pulse processing.

In this paper, a simple structure is proposed to obtain large GVD of the fiber based on an asymmetric dual-core fiber consisting of one core in the center and a neighboring core composed of silica with different refractive indexes and core sizes, respectively. Meanwhile, the proposed asymmetric dual-core fiber (ADCF) provides a freedom in designing the mode diameters of 8—9 μm for the FM in the center core, which is helpful in obtaining mode matching between the ADCF and other spliced SMF. The properties of the ADCF including the GVD, nonlinear parameter and confinement loss, are presented, where the influences of the refractive indexes of the two cores and geometric parameters including the core diameters and the spacing between the two cores on the GVDs are analyzed. Furthermore, the applications of the proposed ADCF are discussed by numerical simulations.

Fig.1 shows the cross section of the ADCF, where the host material is pure silica represented by gray color, the spacing between the centers of the cores is S, the refractive indexes of the cores A (yellow) and B (blue), i.e., n_A and n_B, are dependent of the GeO_2 concentration Xmol%, and d_A and d_B represent the diameters of the cores A and B. The refractive index of the core A is lower than that of the core B to ensure the single-mode and multimode operations in the core A and core B, respectively. According to the coupled mode theory[13], the ADCF can be divided into

* This work has been supported by the National Natural Science Foundation of China (No.61575018).

** E-mail: chcwang@bjtu.edu.cn

two waveguides, i.e., waveguide 1 (W1) with the core A and waveguide 2 (W2) with the core B, respectively. The mode coupling between the cores A and B in the ADCF can occur in the vicinity of index-matched wavelengths, where the propagation modes in two individual waveguides have the same effective refractive index[14]. This dual-core structure intrinsically propagate two supermodes similar to a directional coupler[4,15]. Supermodes are eigenmodes of composite structures involving coupled constituent elements, each of which also supporting guided modes in isolation[16,17].

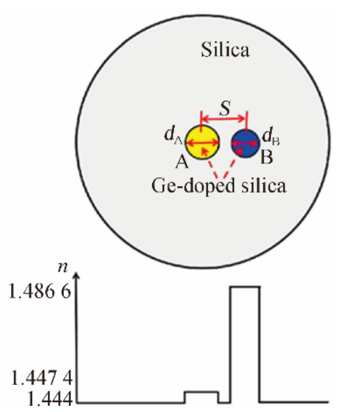

Fig.1 Cross section of the ADCF, where the refractive indices of the cores and cladding are given below the structure diagram

The material dispersions for the pure silica and Ge-doped silica are taken into account in the simulations by using the full-vector finite element method (FVFEM) solver Comsol. The refractive indexes in the pure silica and Ge-doped silica, i.e., n_{cladding} and $n_{\text{A, or B}}$, are given by[18]

$$n_{\text{cladding}}^2 = 1 + \sum_{i=1}^{3} \frac{SA_i \lambda^2}{\lambda^2 - SL_i^2}, \tag{1}$$

$$n_{\text{A, or B}}^2 = 1 + \sum_{i=1}^{3} \frac{\left(SA_i + X\left(GA_i - SA_i\right)\right)\lambda^2}{\lambda^2 - \left(SL_i + X\left(GL_i - SL_i\right)\right)^2}, \tag{2}$$

where the values of parameters SA_i, SL_i, GA_i and GL_i are Sellmeier coefficients[18]. The value of X is the GeO_2 concentration in mol%.

The GVD parameter $D(\lambda)$ in the fiber is given by

$$D(\lambda) = -\frac{\lambda}{c} \frac{\mathrm{d}^2 \operatorname{Re}\left(n_{\text{eff}}\right)}{\mathrm{d}\lambda^2}, \tag{3}$$

where $\operatorname{Re}(n_{\text{eff}})$ is the real part of the effective refractive index n_{eff} at the operating wavelength λ, c is the velocity of light in vacuum.

Since the mode intensity distributes in the Ge-doped silica areas with the different nonlinearity refractive index (NRI) $n_2(x, y)$, the nonlinear parameter $\gamma(\lambda)$ can be defined as

$$\gamma(\lambda) = \frac{2\pi}{\lambda} \frac{\iint_{-\infty}^{\infty} n_2(x,y) \left|F(x,y)\right|^4 \mathrm{d}x\mathrm{d}y}{\left(\iint_{-\infty}^{\infty} \left|F(x,y)\right|^2 \mathrm{d}x\mathrm{d}y\right)^2}, \tag{4}$$

where $F(x, y)$ is the modal intensity distribution of the fiber mode, and the NRIs in the silica and Ge-doped silica part are 2.2 and $(2.2+0.33X)$ with units of 10^{-20} $\mathrm{m^2/W}$[19].

The confinement loss $L_C(\lambda)$ of the modes in the ADCF can be defined by

$$L_C(\lambda) = \frac{20}{\ln(10)} \frac{2\pi}{\lambda} \operatorname{Im}\left(n_{\text{eff}}\right), \tag{5}$$

where $\operatorname{Im}(n_{\text{eff}})$ represents the imaginary part of n_{eff}.

As shown in Fig.2, the waveguide W1 supports only a pair of orthogonally polarized FMs, i.e., x- and y-polarized modes HE_{11}^x and HE_{11}^y, while the waveguide W2 can support the FMs (HE_{11}^x and HE_{11}^y) and HOMs, that are the modes TE_{01}, TM_{01}, HE_{21}, EH_{11}, HE_{31}, HE_{12}, EH_{21}, HE_{41}, HE_{22}, TM_{02} and TE_{02} in the sequence. The important point to note is that, three intersections of the n_{eff} curves between the FMs HE_{11} for the W1 and the higher-order modes TE_{02}, TM_{02} and HE_{22} for the W2 can be obtained near the wavelength window of 1 550 nm by properly tuning the fiber parameters, that correspond to λ=1 550 nm for the mode HE_{22}, 1 551.3 nm for TM_{02} and 1 554.4 nm for TE_{02}, respectively. As a result, the mode coupling between the cores A and B in the ADCF occurs in the vicinity of 1 550 nm. As shown in Fig.3(a), a noteworthy feature is that when the wavelength is increased and close to 1 550 nm, the values of n_{eff} for the supermodes 1 and 2 in the ADCF deviates from n_{eff} curves of higher-order modes (W2) and FMs (W1) due to the enhanced mode coupling effects between them, and then coincide with the n_{eff} curves of the FMs and higher-order modes asymptotically with a further increase in the wavelengths. Since the FMs HE_{11} are polarized in two orthogonal directions, the supermodes can be divided in two cases according to the mode fields with the x- and y-polarization in the core-A region. The former case corresponds to the mode couplings occur between the modes HE_{11}^x and TM_{02}, and HE_{11}^x and HE_{22}, while the latter case corresponds to the couplings between the HE_{11}^y and TE_{02}, and HE_{11}^y and HE_{22}, which are expressed by the forms of 'HE_{11}+TE_{02}' and 'HE_{11}+HE_{22}'. Since the mode intensity distributions of the supermodes with the x-polarized HE_{11}^x in the core A is similar to the case for the y-polarized HE_{11}^y, only the latter case is shown in Fig.3(b), where the mode intensity profiles of the supermodes 1 and 2 are shown at 1 540 nm, 1 550 nm and 1 560 nm, respectively. Furthermore, as shown in Fig.3(c), the absolute values of the GVD for the supermodes 1 and 2 increase dramatically and symmetrically in the vicinity of 1 550 nm because of the mode-coupling-induced waveguide dispersion[15]. The supermodes 1 and 2 exhibit large dispersion characteristics in the normal and anomalous GVD regimes, respectively. A noteworthy feature is that the absolute values of GVD attain its maximum values at the index-matched wavelength, which can also be called the maximum dispersion wavelength (MDW). For example, the values of GVD at the MDW for the supermodes 1 and 2 are −3 942 ps/(nm·km) and 3 040 ps/(nm·km), which are much larger than the GVD of the W1 at 1 550 nm, i.e., 17 ps/(nm·km).

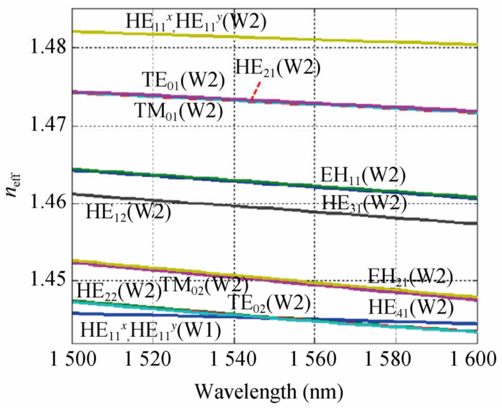

Fig.2 The curves of the effective refractive index n_{eff} for the modes in the W1 and W2

Furthermore, as shown in Fig.3(d), the values of the nonlinear parameter $\gamma(\lambda)$ are less than 0.001 5 W^{-1}/m in the wavelength range of 1 500—1 600 nm, and reduced to below 0.000 6 W^{-1}/m at the MDW. Such low nonlinear parameter ensures that the evolutions of pulse along the fiber are less affected by the nonlinear effects. Additionally, as shown in Fig.3(e), the confinement loss $L_C(\lambda)$ of supermode 1 remains below 1.8×10^{-7} dB/m. The supermode 2 tends to cut off when the wavelength is more than 1 572 nm, where the loss of higher-order modes increases to 0.002 dB/m.

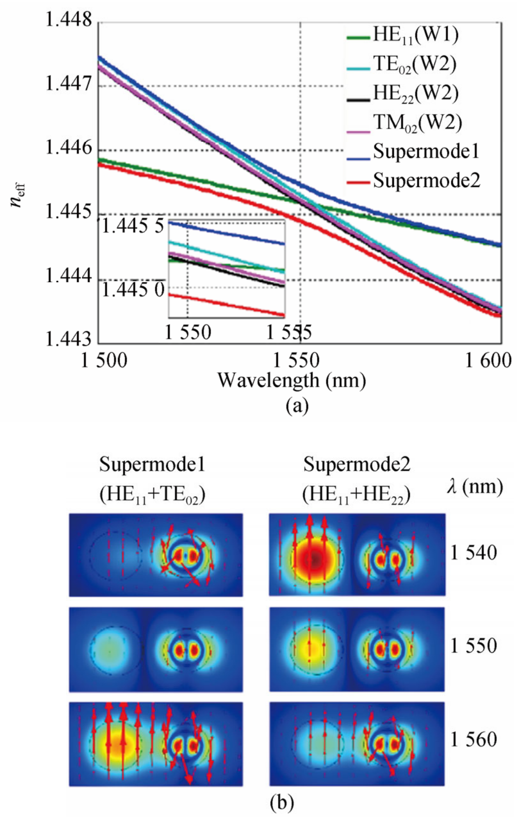

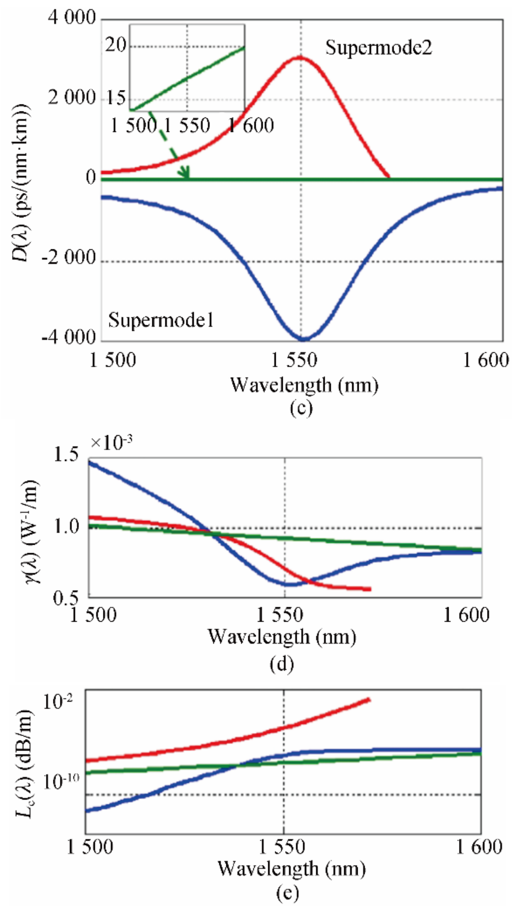

Fig.3 (a) The curves of the n_{eff} of the FMs HE_{11} in the W1, modes HE_{22}, TM_{02} and TE_{02} in the W2, and the supermodes 1 and 2 for the ADCF versus wavelengths λ, where S=12 μm, d_A=9 μm, d_B=8 μm, n_A=1.447 4 and n_B=1.486 6 (when λ=1 550 nm); (b) The mode intensity distributions of the supermodes 1 and 2 at wavelengths of 1 540 nm, 1 550 nm and 1 560 nm; (c) The GVD $D(\lambda)$, (d) nonlinear parameters $\gamma(\lambda)$ and (e) confinement losses $L_C(\lambda)$ for the FMs HE_{11} in the W1, supermodes 1 and 2 in the ADCF, respectively

For the large GVD ADCF, it is important to shift the MDW by tuning the fiber parameters. It can be seen from Fig.4(a) that when the values of d_B increase from 7.9 μm to 8.1 μm and the other parameters remain unchanged, the MDWs shift from 1 530 nm to 1 572 nm. As shown in Fig.4(b), when the values of S increase from 11 μm to 13 μm, the GVD curves for both the supermodes 1 and 2 exhibit an increase in the absolute values of GVD at the MDW accompanied with a narrowing of the GVD profile, and the values of the maximum normal and anomalous dispersion increase from −2 889 ps/(nm·km) and 2 085 ps/(nm·km) to −5 352 ps/(nm·km) and 4 292 ps/(nm·km). Except for the diameters and spacing of two cores, the influence of refractive indexes in the cores A and B on the GVDs of the supermodes 1 and 2 are shown in Fig.4(c) and (d). When the GeO_2 concentrations increase in the cores A and B, the curves of $D(\lambda)$ for the supermodes have blue and red shifts in the wavelength regions, respectively. Therefore, the ADCF with the large GVD and a desired MDW can be obtained by properly tuning geometric parameters and GeO_2 concentrations in the cores A or B.

The designed ADCFs have large values of the GVD and such low nonlinear parameters and confinement losses in 1 550 nm window, especially for the supermode 1 operating in the normal dispersion regime. The result implies an application of the ADCF, i.e., pulse broadening with dispersion compensations. The pulse evolutions along the fiber can be described through solving the generalized nonlinear Schrödinger equation (GNLSE)[19]:

$$\frac{\partial A}{\partial z}+\frac{\alpha}{2}A-\sum_{k\geq 2}\frac{\mathrm{i}^{k+1}}{k!}\beta_k\frac{\partial^k A}{\partial T^k}=\mathrm{i}\gamma\left(1+\mathrm{i}\frac{\partial}{\partial T}\right)\times\left[A(z,T)\int_{-\infty}^{\infty}R(T')\left|A(z,T-T')\right|^2\mathrm{d}T'\right], \quad (6)$$

where $A(z, T)$ is the slowly varying amplitude of the pulse envelope in the time domain, T is the retarded time for a comoving frame at the envelope group velocity $1/\beta_1$, α is the linear loss, β_k are the dispersion coefficients associated with the Taylor series expansion of the propagation constant $\beta(\omega)$ around the center frequency ω_0. In the process of solving GNLSE, the dispersion operator in the frequency domain is applied through multiplication of the complex spectral envelope $\tilde{A}(z, \omega)$ by the operator $\beta(\omega)-(\omega-\omega_0)\beta_1-\beta_0$. The nonlinear response function $R(T)=(1-f_R)\delta(T)+f_R hR(T)$ includes both instantaneous and delayed Raman contributions. The fractional contribution of the delayed Raman response to nonlinear polarization f_R is taken to be 0.18. In the following simulations, the initial pulse is set to be a linearly chirped Gaussian pulse $A_0(T)=\sqrt{P}\exp\left(-(1+\mathrm{i}C)T^2/2T_0^2\right)$,where $T_0=T_{\mathrm{FWHM}}/2\sqrt{2\ln 2}$, and T_{FWHM} is the full width at half maximum (FWHM) pulse duration, C is a chirp parameters, and C=0 for an initially unchirped Gaussian pulse. The peak power P_0 can be obtained by $P_0=0.94E_0/T_{\mathrm{FWHM}}$, where E_0 is the pulse energy. The dispersion length L_D and the nonlinear length L_{NL} are given as

$$L_D=\frac{T_0^2}{|\beta_2|}, \quad (7)$$

$$L_{NL}=\frac{1}{\gamma P_0}, \quad (8)$$

where β_2 is the second-order dispersion. Depending on the relative magnitudes of L_D, L_{NL}, and the fiber length L, either dispersive or nonlinear effects may dominate along the fiber.

Since the supermode 1 of the ADCF can provide large normal GVD, the fiber can offer a potential application in the pulse stretcher. A selective excitation of the supermode 1 can be realized by tapering the ADCF at both ends

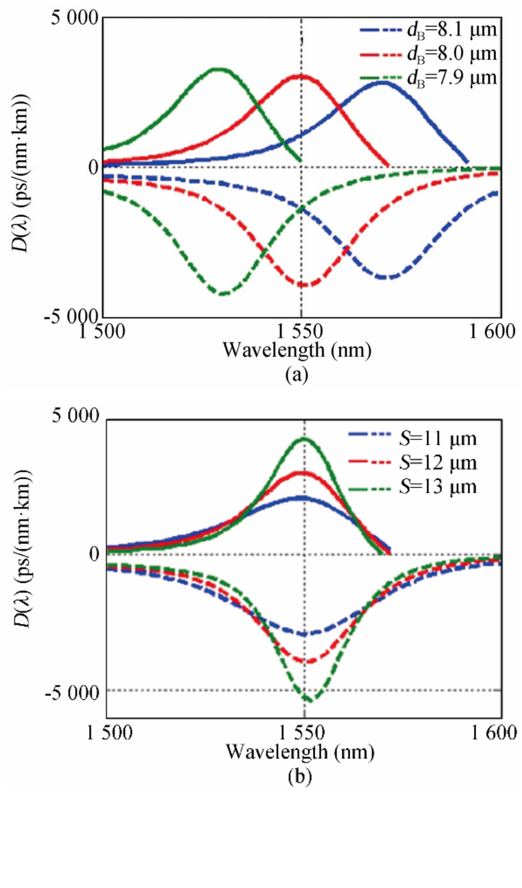

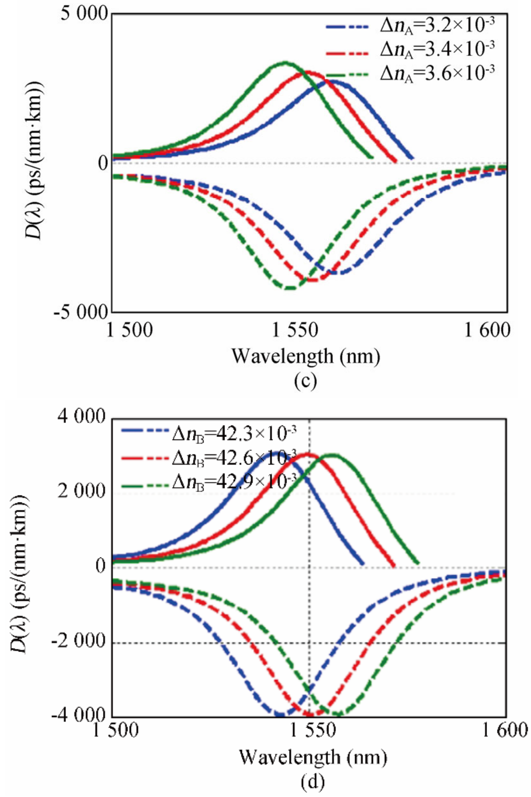

Fig.4 The curves of GVD $D(\lambda)$ for different values of (a) d_B, (b) S, (c) Δn_A and (d) Δn_B, where $\Delta n_A=n_A-n_{silica}$ and $\Delta n_B=n_B-n_{silica}$ represent the index differences between the cores A, B and pure silica, and the curves of GVD $D(\lambda)$ for supermodes 1 and 2 are represented by dashed and solid lines

so that at the splice between the SMF and ADCF, the ADCF supports only the supermode 1[4,20]. The supermode 1 can also be excited by use of optical sources with short temporal coherence lengths[21]. And the supermode 2 appears to suffer a high transmission loss with propagation and virtually becomes cutoff as the wavelength increases. If the fiber length is short enough, the excited supermode 1 can propagate over long lengths with negligible mode coupling[21,22]. As shown in Fig.5, when the unchirped Gaussian pulses input the ADCF and propagate as the supermode 1, the pulse can be broadened by the effects of large normal GVD. For example, the output pulse can be temporally broaden monotonically when the pulse width T_{FWHM} of the 1-nJ input pulse are 0.5 ps and 1 ps. In the case of T_{FWHM}=0.5 ps, the nonlinear length L_{NL} is 0.89 m, the dispersion length L_D is 0.036 m. When L increases from 10L_D to 30L_D, L is much shorter than L_{NL}. Thus the GVD-induced pulse broadening dominates the process of the pulse evolution. The 0.5- and 1-ps pulse can be broaden to 15.5 ps and 30.5 ps when L=30L_D. For the 0.1-ps input pulse with L_D=0.001 4 m and L_{NL}=0.18 m, the intensity profile of the output pulse has a nearly square shape mainly because of the combined effects of the normal GVD and self-phase modulation (SPM).

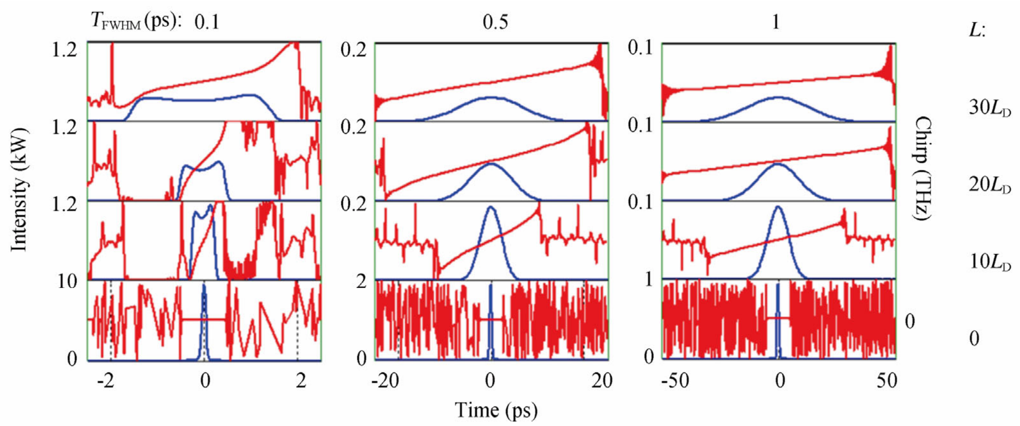

Fig.5 The intensity and chirp profiles of the input and output pulses at the end of the ADCF with different lengths *L* when initial pulse width T_{FWHM}=0.1, 0.5 and 1 ps, for the initial pulse, λ_0=1 550 nm and E_0=1 nJ

For the purpose of estimating the efficiency of pulse broadening, the broadening factor F_b can be defined as

$$F_b = \frac{T^b_{FWHM}}{T_{FWHM}}, \tag{9}$$

where T^b_{FWHM} is the FWHM pulse duration of the broadened pulse.

As shown in Fig.6(a), with the increase of the fiber length L, the values of F_b increase linearly and can reach 31.5 when L=30L_D. Moreover, the values of F_b remain nearly unchanged when the pulse energy increases from 1 nJ to 1 000 nJ mainly because the fiber with a low nonlinear parameter is so short that the nonlinear effects are negligible. For this reason, the broadened pulse has a linearly chirp across the entire pulse even when the pulse energy E_0 reaches 1 000 nJ shown in Fig.6(b).

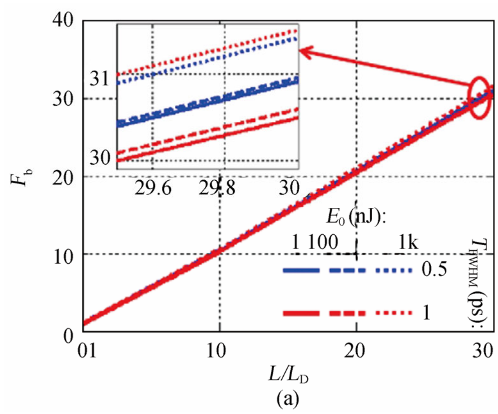

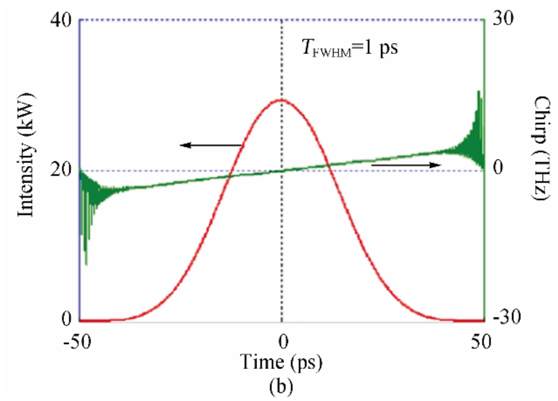

Fig.6 (a) Variation of pulse broadening factor F_b for different values of pulse energy E_0 and T_{FWHM} as a function of L/L_D; (b)The intensity and chirp profiles of the output pulse for the 1-ps pulse with pulse energy E_0=1 000 nJ when L/L_D=30

An approach based on the ADCF is proposed to obtain the large GVD in the fiber. The supermodes in the ADCFs with appropriate parameters can exhibit concave dispersion profiles with large normal and anomalous GVD in the wavelength window of 1 550 nm, where the values of GVD at the MDW are −3 942 ps/(nm·km) and

3 040 ps/(nm·km) in the normal and anomalous dispersion regimes, respectively. At the same time, the values of the nonlinear parameter $\gamma(\lambda)$ can be reduced below 0.001 5 W^{-1}/m in the wavelength range of 1 500—1 600 nm, especially 0.000 6 W^{-1}/m near the MDW. Moreover, the MDW can be shifted over a wide wavelength range by properly tuning the diameter and spacing of the cores and GeO_2 concentrations in the cores A or B. Furthermore, the applications of the ADCF are discussed in the normal GVD regimes by numerically solving the GNLSE. The output pulse can be temporally broaden monotonically as the fiber length increases, and the broadened pulses remain nearly undistorted with increasing pulse energies due to the low nonlinearities and short fiber lengths for the ADCFs.

References

[1] Kivistö S, Herda R and Okhotnikov O G, Optics Express **16**, 265 (2008).

[2] Hill K O, Bilodeau F, Malo B, Kitagawa T, Theriault S, Johnson D C, Albert J and Takiguchi K, Optics. Letters **19**, 1314 (1994).

[3] Kashyap R, Chernikov S V, McKee P F and Taylor J R, Electronics Letters **30**, 1078 (1994).

[4] Thyagarajan K, Varshney R K, Palai P, Ghatak A K and Goyal I C, IEEE Photonic Technology Letters **8**, 1510 (1996).

[5] Gérôme F, Auguste J L, Maury J, Blondy J M and Marcou J, Journal of Lightwave Technology **24**, 442 (2006).

[6] Sakamoto T, Matsui T, Tsujikawa K and Tomita S, Applied Optics **50**, 2979 (2011).

[7] Fujisawa T, Saitoh K, Wada K and Koshiba M, Optics Express **14**, 893 (2006).

[8] Zografopoulos D C, Vázquez C, Kriezis E E and Yioultsis T V, Optics Express **19**, 21680 (2011).

[9] Maji P S and Chaudhuri P R, Optics Communications **325**, 134 (2014).

[10] Yang Si-gang, Zhang Ye-jin, Peng Xiao-zhou, Lu Yang, Xie Shi-zhong, Li Jin-yan, Chen Wei, Jiang Zuo-wen, Peng Jing-gang and Li Hai-qing, Optics Express **14**, 3015 (2006).

[11] Xu Huizhen, Wang Xiuling, Huang Xiaojing, Zhou Changjie, Zhu Huili and Cai Xiaomei, IEEE Photonics Technology Letters **30**, 1499 (2018).

[12] Wei Wei, Zhang Xia, Huang Yong-qing and Ren Xiaomin, Optik **125**, 2749 (2014).

[13] Hardy A and Streifer W, Journal of Lightwave Technology **3**, 1135 (1985).

[14] Li Jie, Mao Yuan, Lu Chao, Hwa Yaw Tam and Wai P K A, Journal of Lightwave Technology **28**, 1608 (2010).

[15] Peschel U, Peschel T and Lederer F, Applied Physics Letters **67**, 2111 (1995).

[16] Kapon E, Katz J and Yariv A, Optics. Letters **9**, 125 (1984).

[17] Xia Cen, Eftekhar M A, Correa R A, Antonio-Lopez J E, Schulzgen A, Christodoulides D and Li Guifang, IEEE Journal of Selected Topics in Quantum Electronics **22**, 1 (2016).

[18] Fleming J W, Applied Optics **23**, 4486 (1984).

[19] G.P. Agrawal, Nonlinear Fiber Optics, Academic Press, San Diego, 2006.

[20] Auguste J L, Blondy J M, Maury J, Marcou J, Dussardier B, Monnom G, Jindal R, Thyagarajan K and Pal B P, Optical Fiber Technology **8**, 89 (2002).

[21] Fermann M E, Optics Letters **23**, 52 (1998).

[22] Bhatia N, Rustagi K C and John J, Optics Express **22**, 16847 (2014).